

## Two Bathointermediates of the Bacteriorhodopsin Photocycle, from Time-Resolved Nanosecond Spectra in the Visible

Andrei K. Dioumaev\* and Janos K. Lanyi

Department of Physiology and Biophysics, University of California, Irvine, Irvine, California 92697

Received: July 31, 2009; Revised Manuscript Received: September 21, 2009

Time-resolved measurements were performed on wild-type bacteriorhodopsin with an optical multichannel analyzer in the spectral range 350–735 nm, from 100 ns to the photocycle completion, at four temperatures in the 5–30 °C range. The intent was to examine the possibility of two K-like bathochromic intermediates and to obtain their spectra and kinetics in the visible. The existence of a second K-like intermediate, termed KL, had been postulated (Shichida et al., *Biochim. Biophys. Acta* **1983**, 723, 240–246) to reconcile inconsistencies in data in the pico- and microsecond time domains. However, introduction of KL led to a controversy, since neither its visible spectrum nor its kinetics could be confirmed. Infrared data (Dioumaev and Braiman, *J. Phys. Chem. B* **1997**, 101, 1655–1662) revealed a state which might have been considered a homologue to KL, but it had a kinetic pattern different from that of the earlier proposed KL. Here, we characterize two distinct K-like intermediates, K<sub>E</sub> (“early”) and K<sub>L</sub> (“late”), by their spectra and kinetics in the visible as revealed by global kinetic analysis. The K<sub>E</sub>-to-K<sub>L</sub> transition has a time constant of ~250 ns at 20 °C, and describes a shift from K<sub>E</sub> with  $\lambda_{\text{max}}$  at ~600 nm and extinction of ~56 000 M<sup>-1</sup>·cm<sup>-1</sup> to K<sub>L</sub> with  $\lambda_{\text{max}}$  at ~590 nm and extinction of ~50 000 M<sup>-1</sup>·cm<sup>-1</sup>. The temperature dependence of this transition is characterized by an enthalpy of activation of  $\Delta H^\ddagger \sim 40$  kJ/mol and a *positive* entropy of activation of  $\Delta S^\ddagger/R \sim 4$ . The consequences of multiple K-like states for interpreting the spectral evolution in the early stages of the photocycle are discussed.

### Introduction

An early, bathochromically shifted, intermediate in the photocycle of bacteriorhodopsin was first detected at cryogenic temperatures<sup>1,2</sup> and called “K”. Later, transient state(s) with similar spectral features in the visible were characterized in kinetic experiments with pico-<sup>3–5</sup> and microsecond<sup>6–9</sup> time resolutions. According to these measurements, the K state is formed at room temperature with a time constant of ~4 ps<sup>4,5,10</sup> and decays to L with a time constant of ~1.2  $\mu$ s.<sup>6,8,9,11–14</sup> Thus, the K intermediate should be a stable and dominating species in the photocycle for more than five decades in time, a feature unique among the known transient states in the photocycles of bacterial rhodopsins. Its predecessor, J, with a lifetime of ~0.5 ps at room temperature,<sup>4,10,15</sup> is believed to be impossible to trap even at 9 K,<sup>16</sup> making K the first intermediate in the photocycle that can be stabilized by low temperature. Further, the rise time of the K state was claimed to be within the picosecond time domain even at 2 K,<sup>3</sup> another unique feature, which suggested a very low barrier to its formation, although this has not been confirmed independently.

Thus, according to long-standing tradition, the same name, K, was used to denote bathochromically shifted state(s) characterized by three different methods: (i) by low temperature trapping and by time-resolved measurements with either (ii) pico- or (iii) microsecond time resolutions. Initially, it was assumed that these three methods characterize one rather than similar but distinct intermediates. Evidence that the assumption of a single state does not hold accumulated as K-like states were characterized by additional instrumental methods. Time-resolved and low temperature measurements in the visible,<sup>17–20</sup> UV,<sup>21,22</sup>

IR,<sup>23–29</sup> resonance Raman,<sup>30–32</sup> CARS,<sup>33</sup> and photoelectric measurements<sup>34</sup> revealed distinct differences between several K-like states created under different conditions and characterized by different methods. From these differences, the concept of a second K-like intermediate emerged.

Shichida et al.<sup>19</sup> calculated a spectrum for a “KL” intermediate between the K and L states (K  $\rightarrow$  KL  $\rightarrow$  L), based on the differences between the difference spectra in the visible measured with 100 ps and 150 ns delays after excitation. The original paper<sup>19</sup> contained no direct information on the rate of K-to-KL conversion. However, others believed that the K-to-KL transition should have a time constant of ~10 ns at room temperature.<sup>12,26,35–37</sup> Extensive studies by several groups failed to detect a transition in this time range,<sup>12,35,36,38</sup> who, therefore, questioned the reliability of the spectral properties implied by the data in ref 19. Thus, on the one hand, the data obtained by a variety of methods did suggest the existence of an additional intermediate between the K state that is formed in picoseconds and L (i.e., a state “homologous” to KL),<sup>17–19,21–27,29–34</sup> but on the other hand, it was shown<sup>35,36</sup> that this state can have neither the spectrum nor the kinetics which would fit the KL state in ref 19. Use of the nonexistent ~10 ns time constant to recalculate spectra from the data sets that did not allow an independent estimate of kinetics<sup>26,27,37</sup> created further confusion.

Later, on the basis of kinetic analysis of time-resolved IR data, an intermediate in the submicrosecond time range was proposed.<sup>29</sup> Its kinetic pattern, decay time at room temperature of ~100 ns<sup>29</sup> rather than ~10 ns, was different from that expected for KL.<sup>19</sup> To highlight the difference of this state<sup>29</sup> from the previously proposed KL state, it was called K<sub>L</sub>, i.e., “late K”, to distinguish it from the “early K”, K<sub>E</sub>, its predecessor. The calculated IR spectra<sup>29</sup> indicated that the absorption

\* To whom correspondence should be addressed. Phone: (949)-824-7783. Fax: (949)-824-8540. E-mail: dioumaev@uci.edu.

maximum of the  $K_L$  state is not as strongly bathochromically shifted as the maximum of  $K_E$ . Existence of  $K_E$  and  $K_L$  as separate intermediates was further supported by time-resolved CARS,<sup>33</sup> in which both the rate constant for the  $K_E$ -to- $K_L$  transition and the main vibrational features of the  $K_E$  and  $K_L$  were shown to be consistent with those in ref 29.

However, there has still been neither visible spectra reported for the  $K_E$  and  $K_L$  states nor a kinetic pattern of their interconversion in the visible, a deficient situation for the photocycle, in which all transitions are customarily characterized as between states defined by their absorption in the visible. The study reported here was performed to close this gap, and we report time-resolved measurements, which yield room temperature spectra of  $K_E$  and  $K_L$  in the visible range, and the kinetics of the  $K_E$ -to- $K_L$ -to- $L$  transitions at ambient temperature.

## Experimental Methods

Wild-type *Halobacterium salinarum* (strain S9) was grown and harvested, and bacteriorhodopsin (in the form of purple membranes) was isolated according to standard procedures.<sup>39</sup> To decrease light scattering, the purple membranes were immobilized in polyacrylamide gel.<sup>40</sup> The gel slices were soaked overnight in 40 mM phosphate buffer at pH 7.0 in the presence of 100 mM NaCl. The sample temperature was controlled with an RTE-111 refrigerated bath/circulator (Neslab, Portsmouth, NH).

The photocycle was initiated by 532 nm flashes of the second harmonics from a Nd:YAG laser (Surelite I, Continuum, Santa Clara, CA) of  $\sim 7$  ns duration, with an energy density of  $<4$  mJ/cm<sup>2</sup> (on the sample), and a repetition rate between 1.25 Hz (at 5 °C) and 5 Hz (at 30 °C). The sample was routinely light-adapted by  $\sim 100$  laser flashes before any measurements; continuous further flashes ensured full light adaptation in the course of the experiment.

Most of the reported time-resolved measurements were performed with an optical multichannel analyzer (OMA) (Princeton Applied Research, Trenton, NJ) equipped with a gated diode array, as described in detail earlier.<sup>41</sup> The measuring light from a 50 W halogen lamp was normally blocked by an optical shutter (model 845, Newport Research, Newport Beach, CA) which was synchronously opened  $\sim 10$  ms before the laser flashes. The testing beam was perpendicular to the excitation beam, and polarized at the “magic angle” ( $54^\circ 44'$ ) relative to the polarization of the excitation to eliminate possible photo-selection artifacts.<sup>42</sup> A full set of data at any temperature consisted of 33 time slices, i.e., time-resolved spectra for the 350–735 nm wavelength range, measured separately for each of the 33 time delays, which were selected on a logarithmic scale to cover the time range from 100 ns to 250 ms with 5–7 time points per decade in time. The gating pulse for the OMA detector was provided with either an FG-100 (for delays  $<400$  ns) or PG-10 pulse generator (both by Princeton Instruments Inc., Trenton, NJ). The exact timing of each time slice (defined as the distance between the laser flash and the center of the OMA gating pulse) was measured with a dual-beam oscilloscope (HP1741A, Hewlett-Packard, Colorado Springs, CO). Each spectrum was measured over time windows of 20 ns for delays shorter than 1.5  $\mu$ s, 150 ns for delays shorter than 15  $\mu$ s, and 1.2  $\mu$ s at longer delays. A total of 400 or 100 flashes were averaged in the case of spectral measurements below and above the 15  $\mu$ s delay time, respectively. Additional data series were measured in a real-time mode on a single-wavelength flash-photolysis setup described previously.<sup>43</sup> The latter are inferior in the crucial (for this study) time region of 100–1000 ns, and

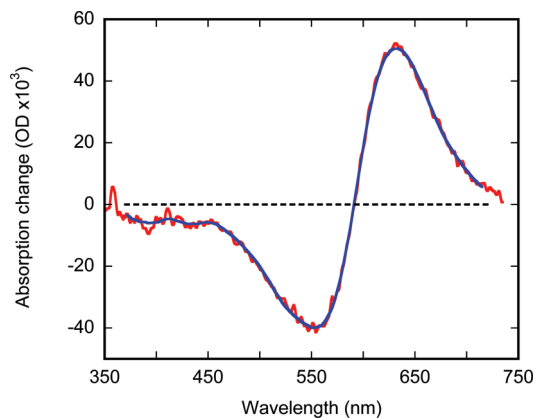


**Figure 1.** Effect of smoothing the measured data with sliding cubic spline. Measured data, red line; smoothed spectrum, blue line. The displayed spectrum was measured with a 100 ns delay after flash. The smoothing results in a 1.8 times decrease in noise.

lack the richness of the OMA spectra, but produce superior kinetic data for the time domain above 1  $\mu$ s.

Bacteriorhodopsin is photodegradable<sup>44,45</sup> in a two-quantum stepwise mechanism<sup>45</sup> that results in a semithreshold behavior, in which pronounced photodamage appears only for flashes of saturation intensity (our unpublished results). Approximately 7500 flashes were used to collect the full data set at each temperature, and even though the excitation flashes' energy was kept below saturation values,<sup>13</sup> this led to a cumulative photodamage with an extent of  $\leq 10\%$ , consistent with ref 45. Under our experimental conditions (nonsaturating flashes), the photodamage linearly increases with the overall number of flashes. To correct for it, a single time slice (e.g., at  $\sim 0.4$  ms delay time for 23 °C) was measured three times—at the beginning, in the middle, and at the end of the data collection—and normalization coefficients between these three data sets were used to apply a linear correction for progressive photodamage in the whole series.

The raw spectra were measured with a  $\sim 1$  nm resolution. Since absorption spectra of bacteriorhodopsin and its intermediates are broad ( $\Delta\lambda_{FWHM} \sim 100$ – $120$  nm<sup>14,46,47</sup>) and nonstructured, for further analysis, each measured spectrum was separately smoothed as in ref 48 by a sliding cubic polynomial over 20 neighboring (i.e.,  $\pm 10$  nm) spectral points, resulting in a data matrix (for each temperature) of 33 time slices by 344 wavelengths. This smoothing decreased the noise level by a factor of 1.8, resulting in an average signal-to-noise ratio of  $\sim 350$  (with “signal” defined as the maximum amplitude of the flash-induced transient depletion at 570 nm). An example of the effect of this smoothing is illustrated in Figure 1 for the first time slice measured with a 100 ns delay.

Kinetic data analysis was performed with a multiexponential global fitting program, *FITEXP*, described earlier.<sup>49</sup> Conclusions on the number of exponentials needed to describe the data on the statistically significant level of confidence were based on *F*-test statistics and on analysis of the residual distribution (see ref 49 for more detail). The *SCHEMEFIT* program<sup>49</sup> was used to calculate temperature-averaged difference spectra of the intermediates, and provided estimates on the extent of influence of the back-reactions.

*MatLab* (The Mathworks, Inc., Natick, MA) and *Kaleida-Graph* (Synergy Software, Reading, PA) software were used for data evaluation and presentation.

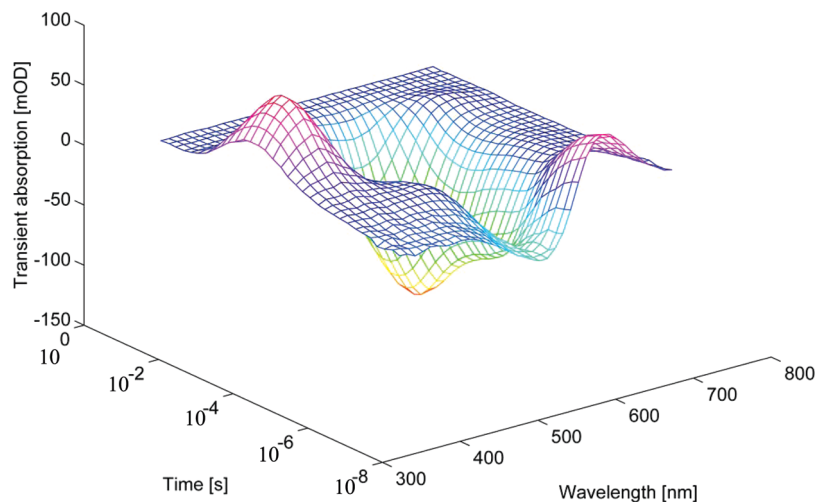


**Figure 2.** 3D plot of flash-induced absorption changes in the photocycle of bacteriorhodopsin at 15 °C. For presentation purposes only, each 10th point in wavelength is shown: a matrix of 36 wavelengths at 33 time points.

## Results

Figure 2 presents a 3D plot of transient absorption changes associated with the bacteriorhodopsin photocycle. Similar data sets were recorded at 5, 15, 23, and 30 °C. Global multiexponential fitting was applied separately for data sets at each temperature, and was performed with three, four, five, six, seven, and eight exponentials. The number of exponentials needed and sufficient for a full kinetic description of the data was estimated from statistical criteria. According to a general theorem of linear differential equations, this number is equal to the number of transient states detected in the experimental series (see, for example, ref 49 for more detail).

Attempts to fit with fewer than five exponentials resulted in poor fits with systematic deviations between the measured data and the correspondent approximation. The five-exponential approximation produced amplitude spectra indicative of the five main intermediates of the photocycle: K, L, M, N, and O (data not shown). At 23 °C, the five apparent exponentials are  $\sim 1 \mu\text{s}$ ,  $\sim 45 \mu\text{s}$ ,  $\sim 130 \mu\text{s}$ ,  $\sim 2.4 \text{ ms}$ , and  $6.8 \text{ ms}$  (in good agreement with published results<sup>8,50,51</sup> on the photocycle kinetics). However, at all temperatures, there remained unreasonably high systematic differences between the measured data and the five-exponential approximation, especially at early times. Increasing the number of exponentials from five to six leads to the appearance of a new, fast component ( $\tau_0 \sim 300 \text{ ns}$  at 23 °C). Its amplitude spectrum is different from that of the next kinetic component ( $\tau_1 \sim 1.3 \mu\text{s}$  at 23 °C), which describes the decay of a later (somewhat similar) K-like state to L (see details and Figure 5 below). The other five time constants were virtually unaffected. Strong systematic deviations at the early times disappear upon inclusion of this sixth exponential (see Figure 3A). *F*-test statistics further confirmed that this sixth exponential is statistically valid (see Figure 3B).

Increase of the number of exponentials, six to seven, further decreased the residual sum of squares. Both the analysis of the residuals (Figure 3A) and the *F*-test statistics (Figure 3B) indicate that the improvement is statistically significant. The additional exponential component, which appears in the seven-exponential approximation, yields an apparent time constant of  $\sim 440 \mu\text{s}$  at 23 °C, in accord with the previous reports.<sup>8,14</sup> Further increase in the number of exponentials, from seven to eight, failed to decrease the residual sum of squares on a statistically significant level (Figure 3B).

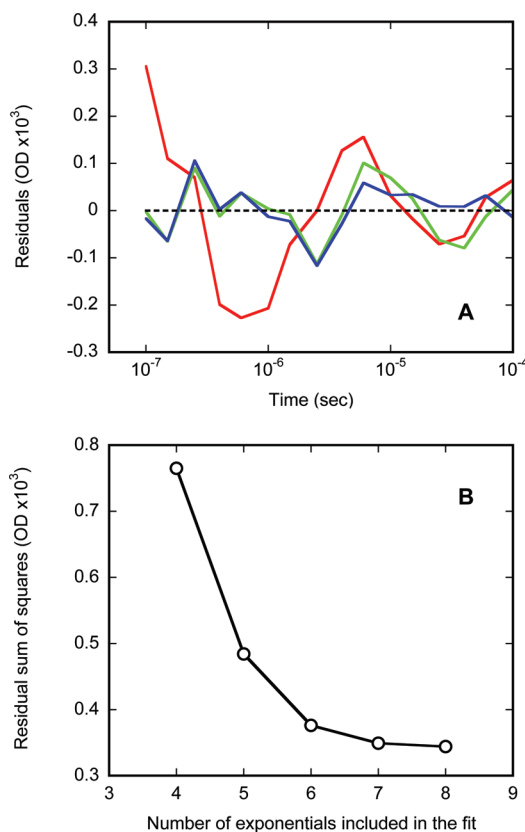


**Figure 3.** Effect of increasing the number of exponentials included in the fit on the residuals. OMA-based data at 15 °C; similar plots were obtained at other temperatures. A: A pronounced decrease in the wavelength-averaged residuals upon inclusion of the  $\tau_0$  component (a difference between the curves in red and green in the time domain below  $10 \mu\text{s}$ ), and absence of further change upon inclusion of the 7th component, which bring improvement only to the time domain above  $\sim 15 \mu\text{s}$  (compare lines in green and blue). B: The residual sum of squares for approximations with increasing number of exponentials.

The risk factor calculated by *F*-test statistics,<sup>52</sup> which reflects the probability of erroneous inclusion of an additional exponential that fails to improve the fit on a statistically significant level, was below 0.05 when the fourth, fifth, sixth, and seventh exponentials were included, but it increased by a factor of  $10^3$  when the eighth component was considered. Thus, our data indicate the presence of seven distinct intermediates, and we



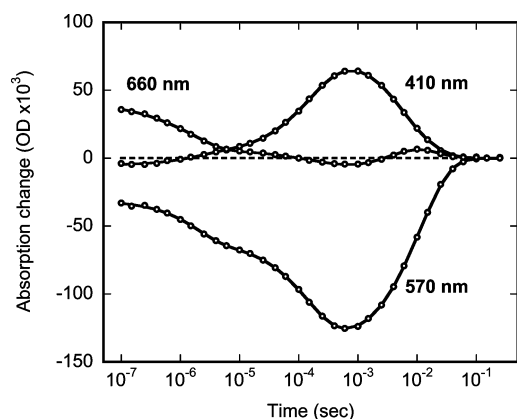


**Figure 4.** Kinetics of absorption changes at 410, 570, and 660 nm reconstructed from 33 time slices measured with OMA at 15 °C (open circles) and the seven-exponential fit (solid lines).

will focus on this seven-exponential approximation below. The data cannot reject the possibility that more than seven intermediates might be present (as has been proposed for example in ref 14), but a six-intermediate description is not sufficient at our signal-to-noise level. Figure 4 presents the kinetic data points at characteristic wavelengths, reconstructed from spectra measured with variable time delays, and the seven-exponential fit is overlaid.

The above analysis was performed separately and independently on each of the data sets measured at different temperatures, and revealed a self-consistent pattern of the presence of at least seven kinetically distinct processes at each of the four measured temperatures, 5, 15, 23, and 30 °C. A table with the fitted time constants at all four temperatures is included in the Supporting Information (Table 1S).

The fastest transition, with a time constant of  $\tau_0 \sim 300$  ns at 23 °C, was not detected previously in any of the time-resolved studies of the photocycle of bacteriorhodopsin in the visible. The appearance of a distinct kinetic component (i.e., of an additional statistically significant exponential) cannot be rationalized in terms of a more complex pattern of interconversions between previously known intermediates but rather signals a detection of a new intermediate on the main path of the bacteriorhodopsin photocycle. Decreasing the temperature to 5 °C increases the corresponding time constant to  $\tau_0 \sim 600$  ns.

A global multiexponential fit results in the so-called apparent rate constants and the amplitude spectra of exponential components. Figure 5A illustrates the corresponding spectral decomposition of the data set at 15 °C with a seven-exponential approximation. The amplitude spectra of exponentials (Figure 5A) are counterintuitive, since they are double-difference spectra, the change during each kinetic component (consecutive exponential) from the previous difference spectrum. To make them easier for visualization, one could reconstruct difference spectra (corrected for the apparent kinetics), which would have been seen in between those kinetic components, i.e., if all of the previous kinetic components were allowed to be completed while the next ones are blocked. For this, each new spectrum (Figure 5B) was calculated as the sum of itself plus all of the spectra of the subsequent processes (Figure 5A). For the photocycle with back-reactions, this representation, shown in Figure 5B, effectively reflects the evolution of the difference spectra between the mixtures of intermediates formed in subsequent exponential processes, and corresponds to the spectra of the so-called “kinetic states”.<sup>14</sup> The first two spectra in Figure 5B reveal that the  $\tau_0$  process accounts for the decay of a strongly

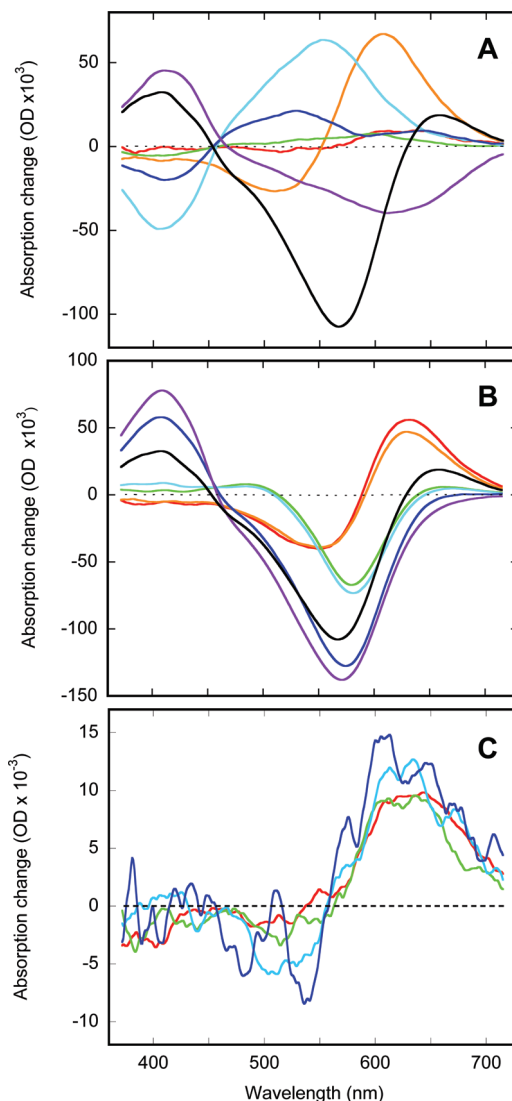


**Figure 5.** Amplitude spectra for the seven-exponential decomposition (by *Fitexp*) of the data in Figure 2. See Table 1 for the time constants. A: Amplitude spectra of all seven kinetic components,  $\tau_0$  (red),  $\tau_1$  (orange),  $\tau_2$  (green),  $\tau_3$  (cyan),  $\tau_4$  (blue),  $\tau_5$  (purple), and  $\tau_6$  (black), respectively. B: Reconstruction of difference spectra of the mixtures of intermediates formed in subsequent exponential processes, i.e., the spectra that would have been observed *before*  $\tau_0$  (red,  $K_E$ ) and *after*  $\tau_0$  (orange, mostly  $K_L$ ), after  $\tau_1$  (green, mostly L), after  $\tau_2$  (cyan, a partial transformation from L to M), after  $\tau_3$  (blue, the main growth of M), after  $\tau_4$  (purple, the maximum of M and some N), and after  $\tau_5$  (black, a partial transformation to O with residual presence of M and N) processes, respectively. Not yet corrected for the presence of back-reactions and the influence of neighboring kinetic processes (see text for details); the difference shown between  $K_E$  and  $K_L$  could only increase upon correction. C: Amplitude spectra of the fastest exponential,  $\tau_0$ , at 5 (red), 15 (green), 23 (cyan), and 30 (blue) °C calculated by *FitExp*.

bathochromically shifted intermediate into the next one, which is characterized by a smaller bathochromic shift. The temperature variations in the amplitude spectra of the fastest component,  $\tau_0$ , are presented in Figure 5C.

The difference spectra in Figure 5B would have corresponded to the true difference spectra if both (i) the exponentials were far apart ( $\tau_i \ll \tau_{i+1}$ ) and (ii) the transitions were unidirectional. Since neither is true for the bacteriorhodopsin photocycle (see Table 1 and refs 53–55), the spectra in Figure 5B have to be corrected for both factors. In the uncorrected form (Figure 5B), they correspond to the difference spectrum of  $K_E$  (first spec-

**TABLE 1: Activation Enthalpies and Entropies and Time Constants<sup>a</sup> at 20 °C, from the Global Fit of Photocycle Kinetics**

	$\tau_0$	$\tau_1$	$\tau_2$	$\tau_3$	$\tau_4$	$\tau_5$	$\tau_6$
time	240 ns	1.2 $\mu$ s	40 $\mu$ s	140 $\mu$ s	400 $\mu$ s	2.6 ms	7.0 ms
constant							
$\Delta H^\ddagger$	43 $\pm$ 15	53 $\pm$ 7	30 $\pm$ 10	38 $\pm$ 8	53 $\pm$ 10	65 $\pm$ 2	67 $\pm$ 3
(kJ/mol)							
$\Delta S^\ddagger/R$	4 $\pm$ 6	6 $\pm$ 3	-9 $\pm$ 6	-5 $\pm$ 3	-6 $\pm$ 4	3 $\pm$ 1	0 $\pm$ 1

<sup>a</sup> Approximate values, recalculated from the temperature dependencies.

trum), which is transformed into a binary mixture of  $K_E$  and  $K_L$  (second spectrum), which is transformed into a tertiary mixture of  $K_E$ ,  $K_L$ , and  $L$  (third spectrum), and so on. The contributions from the early exponentials are not limited to their respective intermediates but are present in the kinetics of concentrations of the later intermediates as well; their contributions diminish with diminishing  $\tau_i/\tau_{i+n}$ . As a result, the amplitude spectra (Figure 5A) of the earlier exponentials are contaminated by spectra of the later processes. The contribution of the later states in the earlier mixtures is decreased with decreasing ratios of  $\tau_i/\tau_{i+n}$  and increases with the more pronounced presence of back-reactions.

The first correction, for the time constants being not sufficiently far apart (for example,  $\tau_1 \approx 5\tau_0$  in our case), is trivial when the apparent time constants are known (see the formula in the Appendix of ref 14, for example). The second correction is not. The presence of back-reactions is evident from the fact that spectra of the seven kinetic processes (as in Figure 5) are similar at different temperatures but not exactly the same (data not shown). To correct for the presence of non-negligible back-reactions, one needs to fit the data not to the formal solution (exponentials) but rather directly to the full system of underlying coupled differential rate equations. The latter (as well as the former) correction was performed with the program *SCHEMEFIT*.<sup>49</sup> It is based on ideas from ref 11, and it simultaneously fits several 2D data matrixes (in time and wavelength) at different temperatures (i.e., a 3D fit), assuming that the kinetics but not the true intermediate spectra are temperature dependent (see refs 55 and 56 for similar attempts). While the full convergence of such a fit of 3D (time, wavelength, and temperature) data set is far from trivial,<sup>49</sup> in our case the early stages of the photocycle were resolved within the first  $\sim 500\,000$  iterations. We will entirely focus here on the early stages; the full analysis of the photocycle will be published elsewhere.

The *SCHEMEFIT* produced temperature-averaged difference spectra of the  $K_E$ ,  $K_L$ , and  $L$  intermediates. These spectra are fully corrected for the apparent kinetics. The corresponding correction for the presence of non-negligible back-reactions is less accurate, since the sensitivity of the data (and therefore the ability for this correction) is limited by the apparent temperature dependence of the calculated amplitude spectra. We consider that the accuracy in the temperature-induced variations of the amplitude spectra of the first component (Figure 5C) is insufficient for defining the  $K_E \leftarrow K_L$  back-reaction, and the  $K_E$ -to- $K_L$  transition was treated as unidirectional. This did not result in any significant temperature dependence of the  $K_E$  spectrum. The  $K_L$ -to- $L$  transition is known to include a non-negligible back-reaction,<sup>48,55–57</sup> and our approximation with *SCHEMEFIT* yielded a ratio of  $\sim 1:3$  for the  $K_L$ -to- $L$  local equilibria, in accord with previous estimates.<sup>48,55–57</sup>

We considered the spectra calculated by *SCHEMEFIT* as the true difference spectra of intermediates, and the absorption

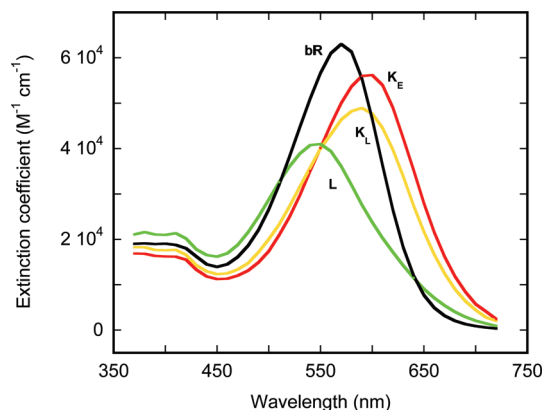


**Figure 6.** Absorption spectra of the  $K_E$ ,  $K_L$ , and  $L$  intermediates calculated by *SCHEMEFIT* (see text). These spectra are temperature-averaged (see text for details).

spectra were then calculated by interactive addition of the absorption spectrum of nonexcited bacteriorhodopsin. The initial estimate for the extent of transformation was obtained by comparing the maximum depletion at 570 nm (Figure 4) to the absorption of the sample. This estimate,  $\sim 15\%$ , is consistent with the estimate from the energy density of excitation flashes<sup>13</sup> (it corresponds to  $\sim 1/3$  of the value obtained with the saturation flashes<sup>13,38</sup>). Further, varying the extent of phototransformation to below 10% or above 20% produced unrealistic absorption spectra, incompatible with our knowledge on photocycle intermediates.<sup>46</sup> Therefore, the spectra shown in Figure 6 were obtained assuming an extent of transformation of 15%.

The gated detector of the OMA-based measuring setup is very effective in eliminating optically induced artifacts from the excitation flash that are potentially serious sources of distortion in the time domain of  $<1\,\mu$ s, vital for our current study. On the other hand, the OMA-based data series has its own limitation, since the cumulative 2D (in time and wavelength) data matrix for kinetic analysis (at a particular temperature) is created by combining separate time slices measured from different excitations, potentially increasing noise in the time direction. The latter might have induced unexpected bias into the kinetic analysis, on which the conclusion of the presence of the  $K_E$ -to- $K_L$  transition relies heavily. As an independent test for the kinetics-based conclusions, we report a kinetic analysis of a complementary time-resolved data set, using a conventional (single-wavelength) flash photolysis setup, which allows measurement of full kinetic curves in real time at selected wavelengths. This mode of measurement has inherently less noise along the time coordinate, which facilitates time-oriented kinetic analysis.

The single-wavelength time-resolved data sets were collected on the same samples at three wavelengths (410, 570, and 660 nm) and five temperatures (5, 10, 15, 20, and 25 °C). A typical result is presented in Figure 7. The five data sets were analyzed by global multiexponential fitting, separately at each temperature (see above for details), yielding for each six statistically significant kinetic components for the time range above 1  $\mu$ s, i.e., after the completion of the  $\tau_0$  process. Finding the same time constants, within the margin of error, independently confirmed the validity of our kinetic analysis of the OMA data. Figure 8 presents the temperature dependence of the fitted time constants from both the OMA-based and single-wavelength measurements. Table 1 presents the apparent activation parameters obtained by a least-squares fit of the Eyring equation<sup>58</sup>

$$\tau = \frac{h}{k \cdot T} \exp\left(-\frac{\Delta S^\ddagger}{R}\right) \exp\left(\frac{\Delta H^\ddagger}{R \cdot T}\right)$$

to the data in Figure 8, and the temperature-averaged time constants recalculated for 20 °C from the fitted values of  $\Delta H^\ddagger$  and  $\Delta S^\ddagger$ . The data from the global six-exponential fit (of the single-wavelength data sets, as in Figure 7) was used for all processes except the  $\tau_0$  one, which is represented by the corresponding data on  $\tau_0$  from the seven-exponential fit on the OMA data.

Since most of the transitions in the photocycle are reversible,<sup>53,59</sup> the calculated time constants and the activation parameters do not correspond to those of the elementary molecular reactions (see more in ref 49), and the temperature dependence is not expected to rigorously obey Eyring's relationship (Figure 8) but merely to follow its general trend due to Boltzman's distribution in fluctuations at the equilibrium.

Because this submicrosecond transition is outside the time domain of most of the previously published kinetic analyses,<sup>8,9,11,14,50,51,55,60–62</sup> our seven-exponential approximation should be compared not to the seven-exponential but rather to the six-exponential approximations in refs 8, 14, 50, 51, 55, 60, and 62. A five-exponential approximation of a data set measured above 1  $\mu$ s results in a kinetic scheme with five "classical" intermediates: K, L, M, N, and O. Within the accuracy of the approximations by different authors,<sup>8,50,51</sup> the

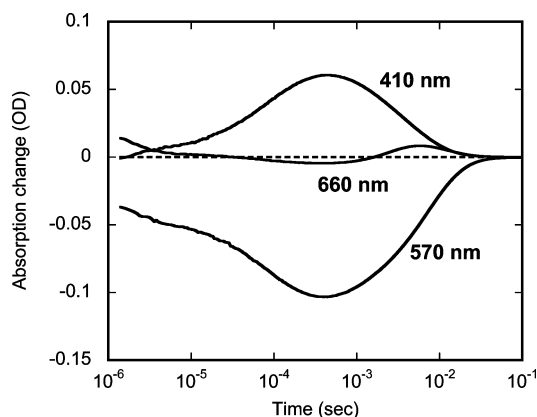


**Figure 7.** Kinetics of absorption changes at 410, 570, and 660 nm measured on a single-wavelength setup at 20 °C.

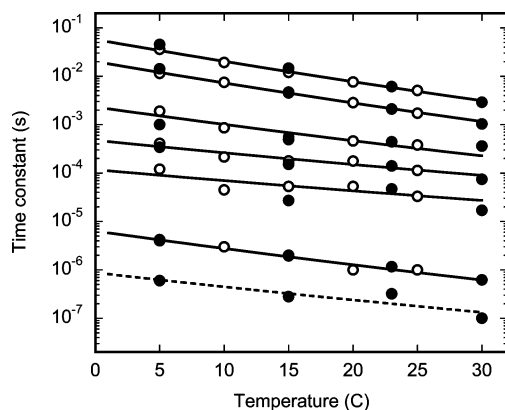


**Figure 8.** Temperature dependence of the seven kinetically distinct components that characterize the flash-induced absorption changes in bacteriorhodopsin. Solid lines: six-exponential global fit approximation of the single-wavelength data (open circles) and its approximation by the Eyring law. Dashed line: approximation, by the Eyring law of the data on  $\tau_0$  (which is not included in the single-wavelength data) from the seven-exponential approximation of the OMA-based data set (filled circles).

apparent time constants at room temperature and neutral pH are  $\sim 1 \mu$ s,  $\sim 50 \mu$ s,  $\sim 150 \mu$ s,  $\sim 2.5$  ms, and  $\sim 7$  ms. Addition of the sixth exponential usually resulted in a time constant of  $\sim 500 \mu$ s<sup>8,14,55,60</sup> and led to a scheme with two M-like intermediates,<sup>55,59,63</sup> which is probably the most-accepted scheme. The values for the six kinetic components in this report (besides the submicrosecond one in the seven-exponential approximation) are fully compatible with these earlier findings.

In our case, the apparent time constant associated with the  $K_E$ -to- $K_L$  transition appeared already at a step when the sixth exponential was included, proving to be even more important for residual sum of squares reduction than the next,  $\sim 500 \mu$ s one, without which the well-established second M-like state would have to disappear from the kinetic scheme (see more in the Discussion).

Instead of multiexponential global fitting, the same data could be analyzed by singular value decomposition, SVD, a matrix method that decomposes the matrix according to the formula  $\mathbf{A} = \mathbf{U} \times \mathbf{S} \times \mathbf{V}^T$  in such a way that the first component presents the best (in the least-squares sense) one-component approximation, the first two components present the best two-component approximation, and so on.<sup>64</sup> When applied to kinetic analysis, SVD decomposes the matrix of absorption changes,  $\Delta A(\lambda, t)$ , into three matrixes: of normalized abstract spectral,  $U(\lambda)$ , and normalized abstract kinetic,  $V(t)$ , components plus a diagonal matrix of singular values,<sup>65</sup> which describe the weights of the contributions of the former two. Conceptually, such decomposition is similar to expanding a function into a series with gradually decreasing (with a decrease in singular values) overall contribution. The product of the first SVD components,  $U(1) \times S(1,1) \times V(1)^T$ , reflects a kinetically weighted average of all absorption changes, while the second and higher components add subsequent order corrections. The first several components do reflect variations in  $\Delta A(\lambda, t)$  due to real kinetics, and their addition progressively improves the quality of data reconstruction until, at some point, the improvement hits the measured noise level, and adding further components begins to reconstruct variations due to noise rather than actual changes. This latter feature enables the use of SVD as noise-filtering utility.

Unlike global fit, SVD does not assume first-order (exponential) kinetics but rather searches for systematic spectral changes with arbitrary kinetics. It has been repeatedly used in kinetic studies both for prefiltering<sup>57,62,66,67</sup> and as a major tool for kinetic analysis.<sup>46,57,62,68–72</sup> To provide directly comparable results, the data in Figure 2 was subjected to SVD. The plot of the corresponding singular values is presented in Figure 9A. The first autocorrelation coefficient, which for the first seven components is 0.99, 0.87, 0.96, 0.89, 0.65, 0.03, and 0.01 correspondingly, is a widely used measure for the nonrandomness, and the component is usually considered valid if the corresponding value is above 0.5 (see, for example, ref 49 for more details). Thus, both the plot of singular values (Figure 9A) and the values of the autocorrelation coefficients indicate that the first five spectral components are responsible for most of the statistically important variations in the data matrix, and their spectra are shown in Figure 9B. The rest of the SVD components, starting from the sixth one, are obscured by noise, making the use of statistical tests on the SVD processes data not quite straightforward; see ref 49 for details. These five components reflect the presence of five spectrally distinct types of spectra, corresponding (most probably) to the K-, L-, M-, N-, and O-like states generally in accord with refs 46 and 57. The fact that the SVD-based analysis seems to favor inclusion of only five components vs seven exponentials (from the global



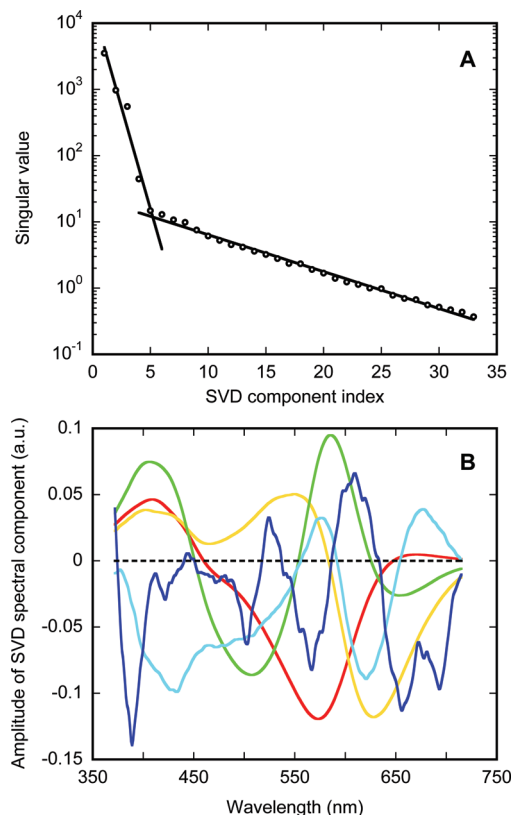


**Figure 9.** Singular value decomposition of the data in Figure 2. A: Plot of singular values (circles), showing a steep decrease with each additional statistically significant component and much slower changes in the singular values that account for noise. The lines are to guide the eye. B: Spectra of the first five components, with unambiguous statistical significance (in red-orange-green-cyan-blue for the first to the fifth component, respectively).

fit) might seem inconsistent. However, the amplitude spectra from the global fit (Figure 7) form a full-rank matrix (i.e., a matrix of the rank of seven), indicating that there is no redundancy in these spectra. The latter reflect a well-known fact that the eigenvectors (amplitude spectra) corresponding to different eigenvalues (exponentials) are linear-independent, and even though exponentials do not form an orthogonal basis, one cannot create any of these seven spectra by linear superposition of the other six. The apparent inconsistency between the ability of the multiexponential fit to extract seven exponentials vs what might seem like a failure of SVD to detect more than five components is rooted in two main factors. First, unlike SVD, which does not assume any particular kinetics, in the global fit analysis the search is restricted to exponential-based kinetics, and this *a priori* information effectively provides a global fit with a competitive advantage over SVD (as long as the assumption of the first-order kinetics holds true). Second, SVD was designed as a rank-reducing algorithm, and it effectively reorganizes the data so that it could be represented with the minimum number of possible components.<sup>64</sup> In the presence of noise, this leads to three distinct types of components in the SVD output: (i) the statistically significant components, which are the first five in our case, (ii) the noise components (most of the rest generated by SVD), and (iii) the components belonging to the “gray zone” between the first two groups. The latter might or might not contain some valid traces of data, but they are masked by noise and are difficult to detect by statistical criteria. The immediate result of this gray zone is that SVD (mis)filtering could easily result in a biased reconstruction; see an illustration in ref 49 for the overfiltering effect.

If the singular values are normalized to their sum, they reflect the fractional contribution of the corresponding components to the data. For the data in Figure 2, the first four components account for 98% of the variation, and each of the next three components adds  $\sim 0.25\%$  each. The fifth component is a valid one based on the autocorrelation test (see above) even though its amplitude spectrum (Figure 9B) looks somewhat noisy because it represents a contribution of only  $\sim 0.28\%$ . Comparing the residual noise level in the seven-exponential approximation (Figure 3B) to the sum of integrals over both light-induced absorption and depletion, one can see that the noise accounts for  $\sim 1.6\%$  of all the variations in data. Therefore, the sixth and seventh (and probably even the eighth) components should be assigned to the “gray zone” (see Figure 9A). SVD rotation was proposed<sup>73</sup> as a method for extracting additional information from such components, but the use of such methods is beyond the aim of this publication.

Globally refitting of the data reconstructed with the first five (the minimal number based on Figure 9A) kinetic traces produced by SVD (i.e., the matrix of  $U \times S$ , in which all of the diagonal elements of  $S$  above 5 are set to zero) with multiexponentials yielded the same seven exponentials as the respective fits of the raw data sets. Thus, SVD analysis produces no evidence against the existence of the seventh distinct kinetic component, on which our conclusion for the two different K-like states,  $K_E$  and  $K_L$  in the  $0.1\text{--}10\ \mu\text{s}$  range, is based. Actually, the same (within the accuracy of the fit) result is obtained even with less than five components. This is not surprising, since the SVD was designed as the rank-reducing algorithm,<sup>64</sup> which effectively redistributes the data to maximize contributions of the statistically valid variations in the first few components. However, this redistribution affects the spectra, and an attempt to globally fit the five-component reconstruction of data yielded a deviation from the fit of the raw data itself: the amplitude spectra were different from those in Figure 5A, reflecting an overfiltering with too few (five) components. This deviation was partially reduced when more than five SVD components were used in reconstruction, confirming that spectral components above the fifth one do contain statistically significant nonstochastic contributions.

## Discussion

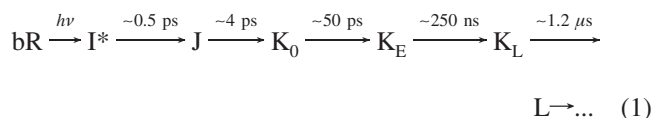
The kinetic analysis revealed the presence of a new kinetic component ( $\sim 240\ \text{ns}$  at  $20\ ^\circ\text{C}$ ), the seventh one in addition to the other six, which correspond to transitions between the six well-established intermediates, K, L,  $M_1$ ,  $M_2$ , N, and O. When the amplitude spectra of these seven components (Figure 5A) were subjected to SVD analysis, it unambiguously indicated that this matrix had the rank of seven, confirming that the seventh component is not a superposition of the other six. *F*-test statistics and residual analysis (Figure 3) confirmed that this new kinetic component is statistically significant and the corresponding improvement in the fit quality could not be due to the increasing number of parameters (and therefore reduced number of degrees of freedom) in the fitted model (seven exponentials vs six). Thus, this new kinetic component represents the seventh eigenvector of the observed kinetics. As it follows from the theory of differential rate equations, this seventh distinct kinetic component unambiguously signals the presence of an extra transient state in addition to the well-established six (K, L,  $M_1$ ,  $M_2$ , N, and O), and *could not* arise from any modification (branching, local equilibria, etc.) of the six-intermediate cycle. Thus, we conclude that our data reveals the presence of a new intermediate,  $K_E$ , with a lifetime of  $\sim 240$

ns at room temperature. This time constant is outside the usual time range (above  $\sim 1 \mu\text{s}$ ), which was routinely covered by the majority of systematic kinetic analysis in the visible.<sup>8,9,11,14,50,51,55,60–62</sup> However, when the time range below  $1 \mu\text{s}$  was included, the corresponding kinetic trace significantly deviated from monoexponentiality between 0.1 and  $5 \mu\text{s}$  (see the trace for the red-shifted intermediate(s) in Figure 10 and its discussion in ref 74), an expected consequence of the  $K_E$  intermediate presence but hard to explain otherwise. Originally, that nonexponentiality was rationalized in terms of the distributed kinetics,<sup>74</sup> but according to our data, the latter could lead to sufficiently strong (as in Figure 10 in ref 74) deviations from exponentiality only below  $\sim 245 \text{ K}$ .<sup>67</sup>

The kinetics of the  $K_E$ -to- $K_L$ -to- $L$  transitions in the visible, which are fully consistent with those from IR,<sup>29</sup> allowed us to decompose the observable transient spectral changes into the spectra of the three distinct intermediates,  $K_E$ ,  $K_L$ , and  $L$  (see Figure 6). As judged by both its spectrum and kinetics, the detected  $K_L$  is equivalent to the well-known  $K$  described by microsecond time-resolved techniques beginning from the midseventies.<sup>6,7</sup> It is, in fact, the last one in the sequence of the  $K$ -like states that precedes the  $L$  intermediate. Its predecessor, which we had termed the  $K_E$  state, and its transition into the  $K_L$  intermediate had not been characterized in the visible. Full spectral and kinetic characterization of the two consecutive  $K$ -like states,  $K_E$  and  $K_L$ , at ambient conditions allows reexamination and rationalization of some earlier results.

First, the early part of the photocycle, after  $J$  but before the  $L$  state, is much more complex than usually believed. The two  $K$ -like states,  $K_E$  and  $K_L$ , distinguishable in the visible, are in agreement with their earlier characterization with time-resolved IR.<sup>29</sup> On the other hand, these cannot be the same as the two  $K$ -like states revealed by low temperature FTIR.<sup>23</sup> The difference between the two  $K$ -like states at cryogenic temperatures, at 81 and 135 K, is primarily in the hydrogen out of plane (HOOP) bands.<sup>23</sup> Comparing the HOOP bands of the two low-temperature  $K$ -like states<sup>23</sup> with those of the two time-resolved  $K$ -like states under ambient conditions,<sup>29</sup> it becomes evident that the “earlier  $K$ ”,  $K_E$ , in the room-temperature time-resolved measurement corresponds to the state trapped at the higher cryogenic temperature, i.e., to what appears to be the “later” one of the low temperature  $K$ 's. Thus, the  $K_E$  and  $K_L$  states we describe in this report are not the first and second but the second and third states in the sequence of at least three consecutive  $K$ -like intermediates. Correspondingly, the changes in the HOOP region reflect the shift between the first ( $K_0$  with HOOP maximum at  $\sim 960 \text{ cm}^{-1}$ ) and the second ( $K_E$  with HOOP maximum at  $\sim 980 \text{ cm}^{-1}$ ) of these three  $K$ -like states not only upon heating from 81 to 135 K<sup>23</sup> but also when the delay in time-resolved measurements is increased from  $10 \text{ ps}^{10}$  to  $10 \text{ ns}$ .<sup>75</sup>

The first part of the cycle, finished with  $L$  formation, contains two conceptually different stages. The first is primary photo-physics, and includes the  $I^*$  and  $J$  states, in which the excess energy from the absorbed photon (and not dissipated on earlier stages) is believed to be still mostly within the electronic system of the retinal (for a review, see refs 76 and 77). The second stage includes at least three consecutive  $K$ -like states, during which the photochemical processes of isomerization and conformational relaxation, most probably, take place. The end-result is the formation of the  $L$  state, in which the usable energy gained from the photon is believed to be at least partially transferred from the retinal into the protein (for a review, see refs 76 and 77). This scheme is the following:



The rates of the rise of the  $J$  state,<sup>4,10,15,78</sup> of  $J$ -to- $K$ ,<sup>4,10,78</sup> and of  $K_L$ -to- $L$ ,<sup>6,8,13</sup> transitions seem to be firmly established, and are not expected to be revised. The combination of this study and the earlier one in the IR<sup>29</sup> has established the spectra and the kinetics of the  $K_E$  state. The  $K_0$ -to- $K_E$  transition has not been characterized in the visible. Its existence is required to reconcile the time-resolved<sup>29</sup> and low-temperature FTIR data.<sup>23,79</sup> A time constant of 40–100 ps was proposed for such a transition based on fast measurements in Raman,<sup>32</sup> IR,<sup>25</sup> and UV.<sup>22</sup> Such a  $70 \pm 30 \text{ ps}^{22,25}$  time constant is consistent with conclusions from the photodamage experiments.<sup>45</sup>

The establishment of two states,  $K_E$  and  $K_L$ , with their distinct differences enables reexamination of some of the spectral inconsistencies from different techniques: (i) at low temperature, (ii) with picosecond resolution, and (iii) with microsecond resolution. At cryogenic temperatures, the  $K$  spectrum ( $K_{77 \text{ K}}$ ) has a difference maximum at  $\sim 645$ , a minimum at  $\sim 550 \text{ nm}$ , and an isosbestic point at  $\sim 595 \text{ nm}$ .<sup>1,2,16</sup> There is no unambiguous way to comparing room-temperature data to that measured at cryogenic temperature. Lowering the temperature from room temperature to 77 K is known to cause a red-shift in the absorption maximum of nonexcited bacteriorhodopsin, by  $\sim 10 \text{ nm}$ .<sup>16</sup> If the corresponding temperature-induced shifts were to be similar for the intermediates, the maximum in the difference spectra of our  $K_E$  at  $\sim 632 \text{ nm}$  and its isosbestic point at  $\sim 589 \text{ nm}$  (see Figure 5) would have been up-shifted if the  $K_E$  were to be measured at 77 K. However, since not only the position of maxima but also the shape of the difference spectra at low temperature are different from those at room temperature,<sup>16</sup> the direct comparison of the difference spectrum of  $K_E$  (in Figure 5) to that of the published spectra of  $K_{77 \text{ K}}$  is hardly feasible.

At room temperature, the published maxima for the  $K$ -like intermediates vary from as low as  $\sim 587 \text{ nm}$  when calculated from data measured with microsecond time resolution (from Figure 5 in ref 46) to as high as  $\sim 605$ – $610 \text{ nm}$  when calculated from picosecond data.<sup>3,78</sup> To minimize the possible bias imposed by additional assumptions involved in calculations, it is more straightforward to compare the directly observed difference spectra instead. For difference spectra measured in the microsecond time domain, the reported maximum is at  $\sim 630 \text{ nm}$  and the minimum is at  $\sim 550 \text{ nm}$ ,<sup>6,41,46,80</sup> as in our data in Figure 5. However, the published isosbestic points are either at 593 nm (calculated from the data in Figure 5 in ref 46 or Figure 2 in ref 80) or at 585 nm (Figure 3 in ref 41) depending on whether<sup>41</sup> or not<sup>46,80</sup> the data for times below  $\sim 300 \text{ ns}$  were considered as well. As we found out, this latter difference reflects the variable presence of the  $K_E$  state vs that of  $K_L$  in the correspondent data sets (that were not corrected for its presence), and is in accord with our current data (see Figures 5 and 6).

For difference spectra measured with 50–100 ps delays, the reported maxima are at 627–635 nm (from Figure 6 in ref 78 and from Figure 2 in ref 3), the difference minima are at 531–542 nm, and the isosbestic points are at 582–584 nm, respectively.<sup>3,78</sup> The picosecond spectra were measured separately at a limited number of wavelengths<sup>3,78</sup> and include considerable uncertainty, and the data, therefore, might be considered generally in accord with our values  $\sim 632$ ,  $\leq 589$  (at 589 before correcting for the kinetics), and  $\sim 551$  (see Figures 5 and 6) for the  $K_E$  state.



Further, the ratio of the positive amplitude in the difference spectra to the amplitude of depletion varies from 1.13–1.15 (calculated from data in Figure 2 in ref 80 and Figure 5 in ref 46) to 1.61–1.84 (Figure 6 in ref 78 and Figure 3 in ref 41, respectively). The lower value of this ratio, 1.13–1.15,<sup>46,80</sup> was obtained from data measured after 300 ns, and corresponds (mostly) to the later one of the two K-like states,  $K_L$ ; it is in accord with a value of  $\leq 1.19$  for the latter. The higher value of this ratio, 1.61–1.84, was obtained from data measured with either 100 ps<sup>78</sup> or 60 ns<sup>41</sup> delays. The value, 1.84 in ref 41, might be overexaggerated due to unnatural shift in the zero-level (compare Figure 3 in ref 41 to our Figure 1 or Figure 3 in ref 46 or Figure 2 in ref 80) and would be decreased to  $\sim 1.3$  if the zero level were readjusted in the 350–450 nm range to that in Figure 1. These values, 1.3–1.61, should be directly comparable with our value of  $\geq 1.37$  for the  $K_E$  state (see Figure 5). We believe that the spectrum of our  $K_E$  state (Figures 5 and 6) is within the errors no different from that of the picosecond K-like when measured either in picoseconds (Figure 6 in ref 78) or early nanoseconds (Figure 3 in ref 41). It has a (calculated) maximum at  $\sim 600$  nm and an extinction of  $\sim 56\,000\text{ M}^{-1}\cdot\text{cm}^{-1}$  (Figure 6). Alternatively, small inconsistencies between the  $K_E$  spectrum in Figure 6 and the spectra measured in picoseconds could be due to the possible presence of the  $K_0$  state.

The calculated spectrum of our  $K_L$  state (Figure 6) is consistent with the published spectra from the measurement with (sub)microsecond time resolution.<sup>6,38,46,80</sup> Its maximum is at  $\sim 590$  nm with an extinction coefficient of  $\sim 50\,000\text{ M}^{-1}\cdot\text{cm}^{-1}$  in good agreement with the  $52\,100\text{ M}^{-1}\cdot\text{cm}^{-1}$  at  $\lambda_{\text{max}} = 586$  nm in ref 46,  $\sim 51\,000\text{ M}^{-1}\cdot\text{cm}^{-1}$  at  $\lambda_{\text{max}} = 587$  nm (from Figure 2 in ref 80), and  $50\,000 \pm 600\text{ M}^{-1}\cdot\text{cm}^{-1}$  at  $\lambda_{\text{max}} = 580 \pm 5$  nm in ref 13.

Third, the substantial activation enthalpy for the  $K_E$ -to- $K_L$  transition ( $\sim 40$  kJ/M) makes it quite sensitive to temperature variations. If extrapolated, the Arrhenius trend (in Figure 8) would require the  $K_E$ -to- $K_L$  transition to be slower than a millisecond at temperatures below 210 K. In the bacteriorhodopsin photocycle, the temperature-induced deceleration is less when the internal kinetics is switched from conventional to distributed below  $\sim 245$  K.<sup>67</sup> Even so, the  $K_E$ -to- $K_L$  transition would be most probably sufficiently slow to explain the observed more than 2 times decrease (when measured on the tens of microseconds time scale) in the magnitude of the K-related photoelectric signal below 200 K.<sup>34</sup> On the other hand, the rise time of the remaining part of the photoelectric signal, the one associated with the  $K_E$  formation, is faster than 5 ns even at  $\sim 90$  K.<sup>34</sup> This very fast rate has to be contrasted with extrapolation from the room temperature Arrhenius trend for  $K_E$  decay that would have led to a time constant of  $\sim 10^{14}$  s at 90 K. The latter estimate is speculative, of course, but indicates that, unlike the decay of  $K_E$  (as well as  $K_L$ ), formation of  $K_E$  seems to be insensitive to temperature. Most probably, this indicates a large difference between the underlying molecular processes during the rise and the decay of  $K_E$ .

There are some clues to what happens during the decay of  $K_E$  in its temperature dependence (Figure 8). While the activation enthalpy,  $\Delta H^\ddagger \sim 40$  kJ/mol, is within the range of the other transitions in the photocycle (30–65 kJ/mol, Table 1), the activation entropy,  $\Delta S^\ddagger/R = 4 \pm 6$ , is somewhat unusual. It is positive, which means that the entropic contribution leads to a decrease in the activation free energy,  $\Delta G^\ddagger = \Delta H^\ddagger - T\Delta S^\ddagger$ , accelerating the transition. The other transitions with positive activation entropies (Table 1) are the  $K_L$ -to-L transition

( $\tau_1$ ) and the one described by the  $\tau_5$  component, which originates mostly from the N-to-O transition. Thus, all transitions in the cycle with positive entropy of activation cluster around events immediately after retinal isomerization. Besides the positive activation entropy, the corresponding states (K-like and O-like) have two more features in common: (i) bathochromic shift of the absorption maxima and (ii) strong HOOP bands in the vibrational spectra,<sup>23,81,82</sup> a feature uncommon for other photocycle intermediates.<sup>81,83</sup> The latter reflects unrelaxed torsional distortion in the chromophore. It is not immediately evident why torsionally distorted states display a decay, which is faster (positive activation entropy) than mandated by the activation enthalpy.

Fourth, the  $K_E$  intermediate, which is predominant on the time scale of tens of nanoseconds, seems to be the best-suited candidate for the state responsible for photodamage. In bacteriorhodopsin, no photodamage occurs under low-intensity continuous illumination<sup>84,85</sup> but irreversible bleaching is observed under intense laser flashes.<sup>44,45,47,86</sup> The latter is characterized by formation of a blue state (max at  $\sim 600$  nm) accompanied by formation of a distinct triple-band structure of the absorption spectrum, at  $\sim 340$ ,  $\sim 360$ , and  $\sim 380$  nm.<sup>44,45,47,86,87</sup> The extent of photodamage is roughly proportional to the square of the absorbed dose,<sup>45,47,86</sup> indicating the involvement of a second photon. However, both the intensity dependence *per se*<sup>45,47</sup> and the estimate of the absorptivity required<sup>47</sup> are inconsistent with a classical nonlinear two-photon mechanism involving a short-lived ( $10^{-15}$ – $10^{-14}$  s) virtual level, which is usually the case in nonlinear optics. Therefore, the second photon has to be absorbed by either J or one of the K-like states. The photodamage caused by nanosecond (10 ns) and picosecond (30 ps) excitation was similar but different from that caused by femtosecond (200 fs) excitation.<sup>45</sup> This implies the involvement of a photocycle intermediate with a lifetime from tens of picoseconds to (at least) tens of nanoseconds but not yet present at times shorter than  $\sim 0.2$  ps. This excludes J and leaves one of the K-like states. The  $K_L$  state has to be excluded also, since its formation is on a submicrosecond time scale, and  $K_L$  is not yet present when a 30 ps flash is used.<sup>45</sup> This leaves the  $K_0$  and  $K_E$  states as candidates. Due to uncertainty in the rate of the  $K_0$ -to- $K_E$  transition,  $K_0$  cannot be completely excluded. However,  $K_0$  could hardly qualify, since a previous extensive search for a transition with a time constant in the range 1–10 ns failed,<sup>12,35,36,38</sup> making  $K_0$  a state too short-lived to be seriously affected by second photon excitation when exposed to the  $\sim 10$  ns flash of the Q-switched laser. Another line of argument is from comparison of the saturation behavior with that of the photodamage, which points out that both processes involve the same state (see more in the Appendix), and for saturation (under nanosecond excitation) this state is definitely  $K_E$ .

In the view of the new kinetic data presented here, we can reassign the spectral features described earlier for K-like intermediates. The spectrum of the K state in ref 3 reflects predominantly  $K_E$  with possible additions of J and  $K_0$ , the one in ref 78 is mostly  $K_E$  with a possible addition of  $K_0$ , and the one in ref 41 is nearly pure  $K_E$ . The K states described in refs 6, 38, and 46 are actually  $K_L$  with possible minor additions of  $K_E$ . The spectrum assigned to “K” in ref 80 is a complex mixture of  $K_E$ : $K_L$ :L in an approximately 15:70:15 ratio. Similarly, the spectrum assigned to the  $K_L$  state in ref 19 is that of an unresolved mixture of  $K_E$ : $K_L$ :L in an approximately 50:45:5 ratio. We believe, therefore, that, to use a generic term, “K intermediate”, for their description is misleading.

## Conclusions

Time-resolved spectroscopy in the visible was used to examine the possibility of a second K-like bathochromic intermediate in the bacteriorhodopsin photocycle under ambient conditions. Global kinetic analysis of a 3D data set in the wavelength, time, and temperature domains revealed two distinct K-like intermediates: the “early”  $K_E$  and the “late”  $K_L$ . Full kinetic deconvolution allowed rationalization of apparent inconsistencies between spectra reported on picosecond and microsecond spectroscopy, which deal predominantly with  $K_E$  and  $K_L$ , respectively.

**Acknowledgment.** The authors wish to thank Dr. Laszlo Zimányi, who built the OMA-based setup at UC Irvine, and Dr. Leonid Brown, who passed the know-how on its use and helped to restart in-house OMA-based measurements. This work was supported in part by grants to J.K.L. from NIH (5R37GM-029498) and DOE (DEFG03-86ER13525).

## Appendix

**Correlation between Photodamage and Saturation Behavior.** Both stepwise photodamage and saturation behavior share the same nonlinear two-quanta mechanism. Saturation, a deviation from the linearity in the Beer law, begins to be noticeable when the photon flux density is increased above the level at which a second interacting photon (from the same flash) could not find a nonphototransformed molecule to interact with but rather meets a molecule that is already excited. On the other hand, at exactly this level of excitation, when the second photon interacts with a phototransformed molecule, the possibility arises that two-quanta photodamage could occur.

Such second-photon interactions become noticeable when the product of the excitation photon flux density ( $I_{\text{flash}}$ ) and the absorption cross-section ( $\sigma$ ) exceeds unity ( $I_{\text{flash}} \cdot \sigma \geq 1$ ). Conversely, saturation occurs at intensities above the critical photon flux density  $I_0 = 1/\sigma$  per flash. In the simplest two-level system (a ground state plus an excited state), the cross section involved is simply the ground state extinction. The latter is defined by the molar extinction coefficient ( $\epsilon$ ), which for most of the organic photochromes is in the range of  $\epsilon \approx 25\,000$ – $250\,000\text{ M}^{-1} \cdot \text{cm}^{-1}$  or in terms of the corresponding absorption cross section  $\sigma \approx 1$ – $10\text{ Å}^2 = (1$ – $10) \times 10^{-16}\text{ cm}^2$ . For the widely used case of an  $\sim 10$  ns excitation flash from the second harmonics of a Nd:YAG laser, the corresponding critical value for the photon density flux,  $I_0$ , is in the range  $I_0 = (0.14$ – $1.4) \times 10^{16}\text{ photons/cm}^2/\text{pulse}$ , which corresponds to  $0.5$ – $5\text{ mJ/cm}^2$  pulses at 532 nm.

Bacteriorhodopsin under nanosecond or picosecond flashes acts rather as a four-level system (the ground and excited states of both bR and  $K_E$  should be taken into account), and the cross section involved in the calculation of the critical photon flux density is weighted, by the quantum yields of the forward ( $\phi_1$ ) and backward ( $\phi_2$ ) reactions, sum of the cross sections of bR ( $\sigma_{\text{bR}}$ ) and  $K_E$  ( $\sigma_{K_E}$ ):  $\sigma = (\phi_1 \cdot \sigma_{\text{bR}} + \phi_2 \cdot \sigma_{K_E})$ .<sup>88</sup> The latter value is in most cases of the same order of magnitude as the ground state absorption. Disregarding correction coefficients due to photoselection<sup>38,42</sup> and to noneven distribution of excitation in optically thick samples,<sup>13</sup> the saturation parameter,  $I_0$ , is  $\sim 4.3\text{ mJ/cm}^2$ , the value measured in ref 13 for bacteriorhodopsin excitation with 532 nm flashes of 10 ns duration. The percentage of cycling molecules ( $A$ ) as a function of excitation energy density ( $I_{\text{flash}}$ ) is characterized by the well-known saturation behavior  $A(I_{\text{flash}}) \sim [1 - \exp(-I_{\text{flash}}/I_0)]$ , and both the significant

deviation in linearity from Beer's law and noticeable photodamage occur when the energy flux density is greater than  $\sim 4.3\text{ mJ/cm}^2$ .

The above estimate for  $I_0$  holds if the state, through which the second-photon interaction takes place, has a lifetime ( $\tau_{\text{decay}}$ ) that is long in relation to the length of the excitation flash ( $\tau_{\text{flash}}$ ) as is the case for the  $K_E$  in bacteriorhodopsin (vs nanosecond excitation). In this case,  $\tau_{\text{decay}}/\tau_{\text{flash}} \gg 1$ , and the saturation curve depends on the energy density only. If, on the contrary, the corresponding state were short-lived, i.e.,  $\tau_{\text{decay}}/\tau_{\text{flash}} \ll 1$ , saturation has to be reached in terms of power density, rather than energy density, and the critical level of photons (per pulse)  $I_0 = 1/\sigma$  has to be corrected by a factor of  $\tau_{\text{decay}}/\tau_{\text{flash}} > 1$ . For example, if the state responsible for photodamage were to decay with a 10 ps time constant, the critical value of  $I_0$  under a 10 ns excitation would increase  $10^3$ -fold, from  $\sim 4 \times 10^{-3}$  to  $\sim 4\text{ J/cm}^2$ . At such levels of energy density, any possible photochemistry will be overshadowed by trivial thermal damage, and the sample would be burned. These considerations result in a well-known rule of thumb: it is next to impossible to saturate a transition that occurs on a time scale much shorter than the pulse length used.

Since under nanosecond excitation photodamage becomes pronounced only when excitation energy density approaches or exceeds saturation intensity (see the results in ref 86, which are confirmed by our own observations), the responsible state should decay on a nanosecond but not picosecond or faster time scale. Therefore, in the view of the kinetics discussed above, the  $K_E$  state seems to be the only candidate.

**Supporting Information Available:** Table showing seven-exponential approximation of the bacteriorhodopsin photocycle at pH 7.0 and figure showing the first measured eight time slices at 15 °C from Figure 1. This material is available free of charge via the Internet at <http://pubs.acs.org>.

## References and Notes

- (1) Stoeckenius, W.; Lozier, R. H. *J. Supramol. Struct.* **1974**, *2*, 769–774.
- (2) Litvin, F. F.; Balashov, S. P.; Sineshchekov, V. A. *Bioorgan. Khim.* **1975**, *1*, 1767–1777.
- (3) Applebury, M. L.; Peters, K. S.; Rentzepis, P. M. *Biophys. J.* **1978**, *23*, 375–382.
- (4) Sharkov, A. V.; Pakulev, A. V.; Chekalin, S. V.; Matveetz, Y. A. *Biochim. Biophys. Acta* **1985**, *808*, 94–102.
- (5) Polland, H. J.; Franz, M. A.; Kaiser, W.; Oesterheld, D.; Zinth, W. *Biochim. Biophys. Acta* **1986**, *851*, 407–415.
- (6) Lozier, R. H.; Bogomolni, R. A.; Stoeckenius, W. *Biophys. J.* **1975**, *15*, 955–962.
- (7) Dencher, N. A.; Wilms, M. *Biophys. Struct. Mech.* **1975**, *1*, 259–271.
- (8) Xie, A. H.; Nagle, J. F.; Lozier, R. H. *Biophys. J.* **1987**, *51*, 627–635.
- (9) Maurer, R.; Vogel, J.; Schneider, S. *Photochem. Photobiol.* **1987**, *46*, 247–253.
- (10) Shim, S.; Dasgupta, J.; Mathies, R. A. *J. Am. Chem. Soc.* **2009**, *131*, 7592–7597.
- (11) Nagle, J. F.; Parodi, L. A.; Lozier, R. H. *Biophys. J.* **1982**, *38*, 161–174.
- (12) Milder, S. J.; Kliger, D. S. *Biophys. J.* **1988**, *53*, 465–468.
- (13) Dioumaev, A. K.; Savransky, V. V.; Tkachenko, N. V.; Chukharev, V. I. *J. Photochem. Photobiol., B* **1989**, *3*, 397–410.
- (14) Chizhov, I.; Chernavskii, D. S.; Engelhard, M.; Müller, K.-H.; Zubov, B. V.; Hess, B. *Biophys. J.* **1996**, *71*, 2329–2345.
- (15) Nuss, M. C.; Zinth, W.; Kaiser, W.; Kolling, E.; Oesterheld, D. *Chem. Phys. Lett.* **1985**, *117*, 1–7.
- (16) Iwasa, T.; Tokunaga, F.; Yoshizawa, T. *FEBS Lett.* **1979**, *101*, 121–124.
- (17) Mao, B. *Photochem. Photobiol.* **1981**, *33*, 407–411.
- (18) Kalisky, O.; Ottolenghi, M. *Photochem. Photobiol.* **1982**, *35*, 109–115.

- (19) Shichida, Y.; Matuoka, S.; Hidaka, Y.; Yoshizawa, T. *Biochim. Biophys. Acta* **1983**, 723, 240–246.
- (20) Balashov, S. P.; Karneeva, N. V.; Litvin, F. F. *Biol. Membr.* **1990**, 7, 586–592.
- (21) Kuschmitz, D.; Hess, B. *FEBS Lett.* **1982**, 138, 137–140.
- (22) Mizuno, M.; Shibata, M.; Yamada, J.; Kandori, H.; Mizutani, Y. *J. Phys. Chem. B* **2009**, 113, 12121–12128.
- (23) Rothschild, K. J.; Roepe, P. D.; Gillespie, J. *Biochim. Biophys. Acta* **1985**, 808, 140–148.
- (24) Braiman, M. S. *Methods Enzymol.* **1986**, 127, 587–597.
- (25) Diller, R.; Iannone, M.; Cowen, B. R.; Maiti, S.; Bogomolni, R. A.; Hochstrasser, R. M. *Biochemistry* **1992**, 31, 5567–5572.
- (26) Weidlich, O.; Siebert, F. *Appl. Spectrosc.* **1993**, 47, 1394–1400.
- (27) Hage, W.; Kim, M.; Frei, H.; Mathies, R. A. *J. Phys. Chem.* **1996**, 100, 16026–16033.
- (28) Sasaki, J.; Maeda, A.; Kato, C.; Hamaguchi, H. *Biochemistry* **1993**, 32, 867–871.
- (29) Dioumaev, A. K.; Braiman, M. S. *J. Phys. Chem. B* **1997**, 101, 1655–1662.
- (30) Hsieh, C.-L.; Nagumo, N.; Nicol, M.; El-Sayed, M. A. *J. Phys. Chem.* **1981**, 85, 2714–2717.
- (31) Hsieh, C.-L.; El-Sayed, M. A.; Nicol, M.; Nagumo, M.; Lee, J.-H. *Photochem. Photobiol.* **1983**, 38, 83–94.
- (32) Doig, S. J.; Reid, P. J.; Mathies, R. A. *J. Phys. Chem.* **1991**, 95, 6372–6379.
- (33) Weidlich, O.; Ujj, L.; Jager, F.; Atkinson, G. H. *Biophys. J.* **1997**, 72, 2329–2341.
- (34) Dioumaev, A. K.; Keszthelyi, L. *Acta Biochim. Biophys. Hung.* **1988**, 23, 271–278.
- (35) Delaney, J. K.; Brack, T. L.; Atkinson, G. H. *Biophys. J.* **1993**, 64, 1512–1519.
- (36) Yamamoto, N.; Ebbesen, T. W.; Ohtani, H. *Chem. Phys. Lett.* **1994**, 228, 61–65.
- (37) Sasaki, J.; Yuzawa, T.; Kandori, H.; Maeda, A.; Hamaguchi, H. *Biophys. J.* **1995**, 68, 2073–2080.
- (38) Dioumaev, A. K.; Tkachenko, N. V.; Chukharev, V. I.; Savransky, V. V. Primary reaction of bathointermediate formation in the bacteriorhodopsin photocycle: quantum yield, photoproduct spectrum and photoinduced reaction mechanism. *Laser Methods in the Studies of Bacteriorhodopsin Photocycle*, Proceeding of IOFAN [38], 53–84. 1992. Moscow, Nauka.
- (39) Oesterhelt, D.; Stoekenius, W. *Methods Enzymol.* **1974**, 31, 667–678.
- (40) Dér, A.; Hargittai, P.; Simon, J. J. *Biochem. Biophys. Methods* **1985**, 10, 295–300.
- (41) Zimányi, L.; Keszthelyi, L.; Lanyi, J. K. *Biochemistry* **1989**, 28, 5165–5172.
- (42) Magde, D. *J. Chem. Phys.* **1978**, 68, 3717–3733.
- (43) Dioumaev, A. K.; Brown, L. S.; Shih, J.; Spudich, E. N.; Spudich, J. L.; Lanyi, J. K. *Biochemistry* **2002**, 41, 5348–5358.
- (44) Govindjee, R.; Balashov, S. P.; Ebrey, T. G. *Biophys. J.* **1990**, 58, 597–608.
- (45) Chizhov, I.; Engelhard, M.; Sharkov, A. V.; Hess, B. *Structure and Function of Retinal Proteins*; John Libbey Eurotext: Paris, 1992; pp 171–173.
- (46) Gergely, C.; Zimányi, L.; Váró, G. *J. Phys. Chem. B* **1997**, 101, 9390–9395.
- (47) Masthay, M. B.; Sammeth, D. M.; Helvenston, M. C.; Buckman, C. B.; Li, W.; Cde-Baca, M. J.; Kofron, J. T. *J. Am. Chem. Soc.* **2002**, 124, 3418–3430.
- (48) Nagle, J. F.; Zimányi, L.; Lanyi, J. K. *Biophys. J.* **1995**, 68, 1490–1499.
- (49) Dioumaev, A. K. *Biophys. Chem.* **1997**, 67, 1–25.
- (50) Hofrichter, J.; Henry, E. R.; Lozier, R. H. *Biophys. J.* **1989**, 56, 693–706.
- (51) Maurer, R.; Vogel, J.; Schneider, S. *Photochem. Photobiol.* **1987**, 46, 255–262.
- (52) Bevington, P. R. *Data reduction and error analysis for the physical sciences*; McGraw-Hill: New York, 1969; pp 1–336.
- (53) Ames, J. B.; Mathies, R. A. *Biochemistry* **1990**, 29, 7181–7190.
- (54) Váró, G.; Lanyi, J. K. *Biochemistry* **1990**, 29, 2241–2250.
- (55) Lozier, R. H.; Xie, A. H.; Hofrichter, J.; Clore, G. M. *Proc. Natl. Acad. Sci. U.S.A.* **1992**, 89, 3610–3614.
- (56) van Stokkum, I. H. M.; Lozier, R. H. *J. Phys. Chem. B* **2002**, 106, 3477–3485.
- (57) Zimányi, L.; Saltiel, J.; Brown, L. S.; Lanyi, J. K. *J. Phys. Chem. A* **2006**, 110, 2318–2321.
- (58) Eyring, H. *Chem. Rev.* **1935**, 17, 65–77.
- (59) Váró, G.; Lanyi, J. K. *Biochemistry* **1991**, 30, 5008–5015.
- (60) Rödig, C.; Chizhov, I.; Weidlich, O.; Siebert, F. *Biophys. J.* **1999**, 76, 2687–2701.
- (61) Hendler, R. W.; Shrager, R. I.; Bose, S. *J. Phys. Chem. B* **2001**, 105, 3319–3328.
- (62) Lorenz-Fonfria, V. A.; Kandori, H. *J. Am. Chem. Soc.* **2009**, 131, 5891–5901.
- (63) Nagle, J. F. *Photochem. Photobiol.* **1991**, 54, 897–903.
- (64) Golub, G. H.; Van Loan, C. F. *Matrix computations*; Johns Hopkins University Press, Baltimore, MD, 1996; pp 1–694.
- (65) Henry, E. R.; Hofrichter, J. *Methods Enzymol.* **1992**, 210, 129–192.
- (66) Lakatos, M.; Lanyi, J. K.; Szakács, J.; Váró, G. *Biophys. J.* **2003**, 84, 3252–3256.
- (67) Dioumaev, A. K.; Lanyi, J. K. *Biochemistry* **2008**, 47, 11125–11133.
- (68) Hessling, B.; Souvignier, G.; Gerwert, K. *Biophys. J.* **1993**, 65, 1929–1941.
- (69) Zimányi, L.; Kulcsar, A.; Lanyi, J. K.; Sears, D. F., Jr.; Saltiel, J. *Proc. Natl. Acad. Sci. U.S.A.* **1999**, 96, 4414–4419.
- (70) Kulcsar, A.; Saltiel, J.; Zimányi, L. *J. Am. Chem. Soc.* **2001**, 123, 3332–3340.
- (71) Groma, G. I.; Kelemen, L.; Kulcsar, A.; Lakatos, M.; Váró, G. *Biophys. J.* **2001**, 81, 3432–3441.
- (72) Shrager, R. I.; Hendler, R. W. *J. Phys. Chem. B* **2003**, 107, 1708–1713.
- (73) Henry, E. R. *Biophys. J.* **1997**, 72, 652–673.
- (74) Borucki, B.; Otto, H.; Heyn, M. P. *J. Phys. Chem. B* **1999**, 103, 6371–6383.
- (75) Kaminaka, S.; Mathies, R. A. *Laser Chem.* **1999**, 19, 165–168.
- (76) Lanyi, J. K. *J. Phys. Chem. B* **2000**, 104, 11441–11448.
- (77) Lanyi, J. K. *Annu. Rev. Physiol.* **2004**, 66, 665–688.
- (78) Polland, H. J.; Franz, M. A.; Kaiser, W.; Kölling, E.; Oesterhelt, D.; Zinth, W. *Biophys. J.* **1986**, 49, 651–662.
- (79) Maeda, A.; Verhoeven, M. A.; Lugtenburg, J.; Gennis, R. B.; Balashov, S. P.; Ebrey, T. G. *J. Phys. Chem. B* **2004**, 108, 1096–1101.
- (80) Goldschmidt, C. R.; Ottolenghi, M.; Korenstein, R. *Biophys. J.* **1976**, 16, 839–843.
- (81) Maeda, A. *Isr. J. Chem.* **1995**, 35, 387–400.
- (82) Smith, S. O.; Pardo, J. A.; Lugtenburg, J.; Curry, B.; Mathies, R. A. *Biochemistry* **1983**, 22, 6141–6148.
- (83) Zscherp, C.; Heberle, J. *J. Phys. Chem. B* **1997**, 101, 10542–10547.
- (84) Bräuchle, C. R.; Hampp, N.; Oesterhelt, D. *Proc. SPIE* **1993**, 1852, 238–242.
- (85) Hampp, N. A. *Chem. Rev.* **2000**, 100, 1755–1776.
- (86) Fischer, T.; Hampp, N. A. *Biophys. J.* **2005**, 89, 1175–1182.
- (87) Czégé, J.; Reinisch, L. *Photochem. Photobiol.* **1991**, 53, 659–666.
- (88) Dioumaev, A. K.; Savransky, V. V.; Tkachenko, N. V.; Chukharev, V. I. *J. Photochem. Photobiol., B* **1989**, 3, 385–395.